

---

# BoHA: Blockwise Hadamard Product Adaptation for Parameter-Efficient Fine-Tuning

---

Feng Yu\* Jia Hu Geyong Min  
Department of Computer Science  
University of Exeter

## Abstract

Parameter-efficient fine-tuning (PEFT) of large language models trains a small task-specific parameter set while keeping the pretrained model frozen. The dominant Low-Rank Adaptation (LoRA) family makes this trade-off practical; however, evaluations under the same parameter budget assess single-task accuracy. In sequential adaptation settings, such evaluations should also measure how well performance on the first-stage task is retained after subsequent fine-tuning. To address this gap, we introduce BoHA, a blockwise  $W_0$ -coupled Hadamard product adapter that treats spatial support as an explicit design axis. BoHA partitions the frozen weight  $W_0$  into a  $b \times b$  grid and learns an independent low-rank Hadamard product factor in each block, preserving a matched LoRA-equivalent total rank with adapter-free merged inference. On a synthetic target, BoHA at per-block rank  $r_b=1$  exactly reconstructs an update that requires rank  $b^2$  under the global  $W_0$ -coupled Hadamard parameterization. Across Llama-3.2-1B/3B, Mistral-7B, and Gemma-2-9B on commonsense and arithmetic reasoning tasks, BoHA outperforms LoRA across all matched-budget single-task averages and remains competitive with the strongest Hadamard baseline. On a Llama-3.2-3B commonsense  $\rightarrow$  arithmetic continual-learning diagnostic, BoHA retains 57.66% first-stage accuracy and exceeds the  $W_0$ -free additive-control mean by 15.23% under matched second-stage plasticity. These results demonstrate that blockwise  $W_0$ -coupled Hadamard adaptation is a competitive PEFT design choice when retention under sequential adaptation is part of the objective.

## 1 Introduction

Adapting large language models by full fine-tuning is costly when one base model must serve many specialized deployments [3, 10]. Parameter-efficient fine-tuning (PEFT) reduces this cost by training a small task-specific parameter set while freezing the pretrained model [15, 16]. The dominant parameterization is Low-Rank Adaptation (LoRA) [16], which adds a low-rank trainable update  $\Delta W$  to the frozen weight  $W_0$ , motivated by the finding that fine-tuning trajectories lie in low-dimensional subspaces [1]. Subsequent PEFT research refines this parameterization along several axes: reweighting or reinitializing the additive update [24, 28], relaxing LoRA’s rank constraint by composing the update multiplicatively with  $W_0$  [18] or via a Hadamard product without coupling to  $W_0$  [37], or imposing block or Kronecker structure on the additive factors [20, 12, 39].

The taxonomy above varies how the additive update is reweighted, decomposed, or block-tiled, while multiplicative coupling to  $W_0$  is either fixed in a single global Hadamard form [18] or removed entirely, leaving the update  $W_0$ -free. These designs are usually compared by fixing trainable parameter count and reporting single-task accuracy. Under sequential adaptation, a later fine-tuning stage can degrade earlier-task performance [27, 22, 9], which matched-budget single-task evaluations do not

---

\*Correspondence: fy274@exeter.ac.uk

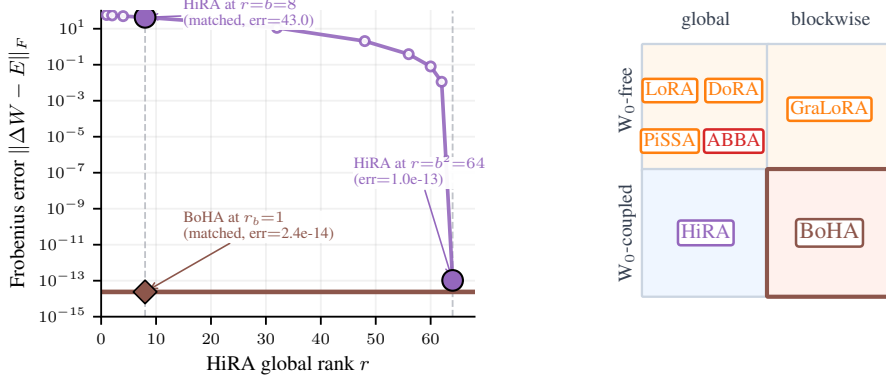


Figure 1: **BoHA synthetic construction and design axes.** (a) On a synthetic target where  $E \oslash W_0$  has per-block rank 1 and global rank  $b^2$ , BoHA reconstructs at  $r_b=1$  while a global Hadamard parameterization needs global rank  $b^2$ . (b) PEFT methods organized by  $W_0$ -coupling and spatial support. BoHA occupies the blockwise  $W_0$ -coupled cell.

capture. This motivates a research question: *how should an adapter allocate its update across a weight matrix when both matched-budget accuracy and retained accuracy after subsequent fine-tuning matter?*

We answer this question by separating two structural axes the single-task protocol leaves implicit:  $W_0$ -coupling (whether  $\Delta W$  is multiplicatively coupled to the frozen weight at evaluation) and spatial support (global vs. blockwise). We introduce Blockwise Hadamard Product Adaptation (BoHA), which combines blockwise support with  $W_0$ -coupled Hadamard modulation: a  $b \times b$  partition of  $W_0$  with an independent low-rank Hadamard product per block, at LoRA-equivalent total rank, as shown in Figure 1(b). The analysis isolates what blockwise localization changes: with  $E$  denoting the full fine-tuning update, BoHA fits the elementwise ratio  $E \oslash W_0$  through per-block approximations at matched LoRA-equivalent total rank. A synthetic target where  $E \oslash W_0$  has per-block rank 1 and global rank  $b^2$  separates this family from a single global Hadamard factorization, as illustrated in Figure 1(a).

Across theory, synthetic reconstruction, matched-budget single-task evaluation, and a commonsense  $\rightarrow$  arithmetic continual-learning diagnostic, the results identify spatial support as a structural axis for  $W_0$ -coupled Hadamard adaptation with measurable retention impact at matched second-stage plasticity. Our main contributions are summarized as follows:

- We identify a global Hadamard parameterization shared by current Hadamard-product PEFT methods and introduce BoHA, a blockwise  $W_0$ -coupled Hadamard product adapter that treats spatial support as an explicit design axis at LoRA-equivalent total rank with no additional inference latency.
- We characterize BoHA through a per-block approximation bound and a gradient-locality property that separate blockwise from global  $W_0$ -coupled Hadamard parameterization.
- On commonsense and arithmetic benchmarks across four base-model scales, BoHA improves over LoRA on every matched-budget single-task average and remains competitive with the strongest Hadamard baseline.
- On a Llama-3.2-3B commonsense  $\rightarrow$  arithmetic continual-learning diagnostic,  $W_0$ -coupled Hadamard adapters occupy the high-retention end of the design space, with BoHA exceeding the  $W_0$ -free additive-control mean by 15.23% at matched second-stage plasticity.

## 2 Preliminaries and Design Axes

PEFT parameterizations for a frozen weight  $W_0 \in \mathbb{R}^{m \times n}$  differ along two structural axes. The first is  $W_0$ -coupling, whether the learned update is parameterized as a multiplicative modulation of the frozen weight, such as  $\Delta W = W_0 \odot H$  for a learned matrix  $H$ . The second is *spatial support*, whether the learned factors span the full matrix or act on disjoint submatrices. We separate  $W_0$ -coupling from

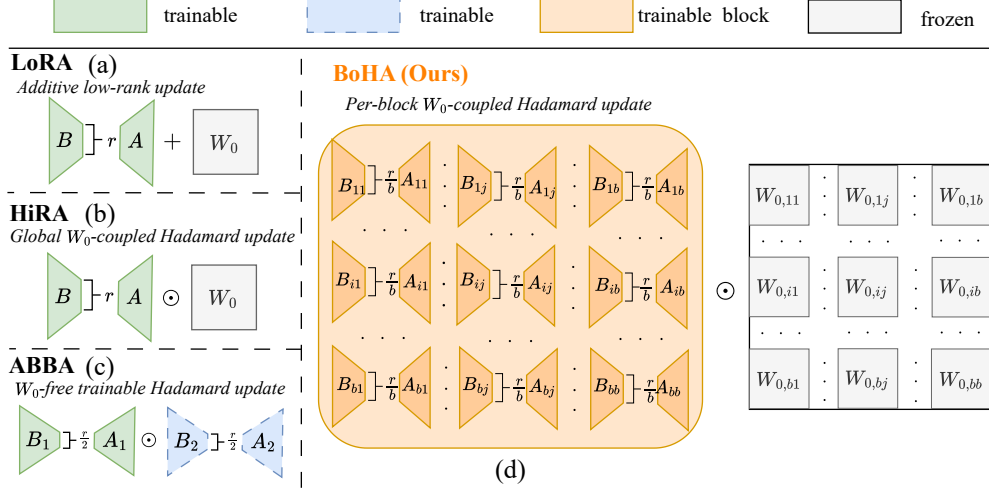


Figure 2: Update parameterizations of LoRA, HiRA, ABBA, and BoHA along the  $W_0$ -coupling and spatial-support design axes. BoHA partitions  $W_0$  into a  $b \times b$  grid and learns an independent  $W_0$ -coupled Hadamard modulation in each block, with  $b = 8$  in our main experiments.

$W_0$ -initialization: PiSSA [28] and ABBA [37] can initialize from singular components of  $W_0$ , but the trained update is merged additively or through trainable factors rather than through  $W_0$  itself, so the coupling does not persist at evaluation.

Under these axes, LoRA [16], DoRA [24], and PiSSA are global,  $W_0$ -free additive updates. ABBA is global and Hadamard but remains  $W_0$ -free because both Hadamard factors are trainable. GraLoRA [20] is blockwise but additive, and HiRA [18] is  $W_0$ -coupled but global. The proposed BoHA occupies the blockwise  $W_0$ -coupled cell by placing an independent low-rank Hadamard product inside each block of a  $b \times b$  partition of  $W_0$ , as shown in Figure 1(b).

The two axes play different roles in our evidence. The forward continual-learning diagnostic compares BoHA with HiRA and with  $W_0$ -free controls, including the blockwise  $W_0$ -free control GraLoRA. The theory below isolates the blockwise approximation effect. Let  $W^*$  denote the full fine-tuning target and  $E = W^* - W_0$  the corresponding update. The global Hadamard parameterization, with HiRA as its  $W_0$ -coupled instance, fits a single rank- $r$  factor pair to the elementwise ratio  $E \oslash W_0$  across the entire layer. When this ratio is low-rank within local blocks but high-rank globally, the global approximation becomes restrictive. BoHA applies the  $W_0$ -coupled approximation within each block, using per-block factors at the same LoRA-equivalent total rank. The synthetic instance in Figure 1(a) illustrates this separation: a global Hadamard parameterization matches the construction only at global rank  $b^2$ , which is  $b$  times BoHA’s LoRA-equivalent total rank in this synthetic example. The next section formalizes this with a blockwise approximation bound and a gradient-locality result.

Tensor-product factorizations such as KronA [12] and LoKr [39] are  $W_0$ -free tensor-structured updates rather than disjoint blockwise  $W_0$  modulations. Related rank-scaling and spectral analyses [21, 36] and parameter-efficient continual fine-tuning methods [8, 23] are surveyed in the related-work appendix.

### 3 Method: Blockwise Hadamard Product Adaptation

For a frozen linear weight  $W_0 \in \mathbb{R}^{m \times n}$ , BoHA parameterizes the trainable update as a  $W_0$ -coupled Hadamard modulation applied independently over a  $b \times b$  block partition. At LoRA-equivalent total rank  $r_{\text{tot}} = br_b$ , with per-block rank  $r_b$ , BoHA exactly matches LoRA’s trainable-parameter count at rank  $r_{\text{tot}}$  and introduces no additional inference latency. Full derivations of the two propositions are in Appendix B. Figure 2 locates BoHA against LoRA, HiRA, and ABBA in the design space of section 2.

**Parameterization.** HiRA [18] represents the update as  $\Delta W_{\text{HiRA}} = W_0 \odot (BA)$  with  $A \in \mathbb{R}^{r \times n}$  and  $B \in \mathbb{R}^{m \times r}$ . Let  $E = W^* - W_0$  denote a full-finetuning target update and  $\odot$  the elementwise

Table 1: Comparison of approximation requirements and algebraic rank bounds for PEFT methods.

Method	rank( $\Delta W$ ) upper bound	Approximation requirement	Dependence on $W_0$
LoRA	$r_{\text{tot}}$	$\text{rank}(E) \leq r_{\text{tot}}$	None
HiRA	$\text{rank}(W_0) \cdot r_{\text{tot}}$	$\text{rank}(E \odot W_0) \leq r_{\text{tot}}$	Global modulation
GraLoRA	$b \cdot r_{\text{tot}}$	per-block $\text{rank}(E_{ij}) \leq r_b$	None
ABBA	$r_1 \cdot r_2$	$\text{rank}(E) \leq r_1 r_2$	None (init only)
<b>BoHA (ours)</b>	$b \cdot \text{rank}(W_0) \cdot r_{\text{tot}}$	<b>per-block</b> $\text{rank}(E_{ij} \odot W_{0,ij}) \leq r_b$	Blockwise modulation

division operator. The HiRA parameterization then approximates the elementwise ratio  $E \odot W_0$  by a single global rank- $r$  product across the entire layer. When this target is low-rank within blocks but high-rank globally, the global factorization can become the limiting approximation, as illustrated in Figure 1(a). BoHA therefore partitions the row and column dimensions of  $W_0$  into a conformal  $b \times b$  grid. The formulation only requires blocks  $W_{0,ij} \in \mathbb{R}^{m_i \times n_j}$  that tile  $W_0$ . We use equal-size blocks in our experiments. For each block  $(i, j)$ , BoHA stores factors  $A_{ij} \in \mathbb{R}^{r_b \times n_j}$ ,  $B_{ij} \in \mathbb{R}^{m_i \times r_b}$ , assembled as

$$\Delta W_{\text{BoHA}} = W_0 \odot \bigoplus_{i,j=1}^b B_{ij} A_{ij}, \quad (1)$$

where  $\bigoplus$  places each  $B_{ij} A_{ij}$  in its  $(i, j)$  tile and  $r_{\text{tot}} = b \cdot r_b$  is the LoRA-equivalent total rank. The trainable parameter count is  $\sum_{i,j} r_b(m_i + n_j) = b r_b(m + n) = (m + n)r_{\text{tot}}$ , matching LoRA at rank  $r_{\text{tot}}$ . The sum of per-block rank capacities is  $b^2 r_b$ , which enters the capacity bound of Table 1 without changing the trainable-parameter count.

This parameterization separates BoHA from the closest PEFT families. Setting  $b=1$  recovers HiRA exactly, and Appendix F reports the corresponding equivalence check. Removing the  $W_0$  factor gives a  $W_0$ -free blockwise additive update, analogous to GraLoRA [20]. ABBA learns both Hadamard factors [37], whereas BoHA keeps the pretrained weight frozen and trains only blockwise low-rank modulations coupled to it.

**Blockwise approximation bound.** Inheriting the partition above,  $E$  admits the conformal partition  $E_{ij}$ . Let  $R_{ij} = E_{ij} \odot W_{0,ij}$  denote the per-block elementwise ratio and  $\|M\|_{\max} = \max_{u,v} |M_{uv}|$  the entrywise maximum-absolute norm. HiRA is the  $b = 1$  special case with  $R = E \odot W_0$ . The bound is most favorable when  $R$  has lower rank within blocks than globally. The next bound replaces one global truncation error with a sum of blockwise truncation errors.

**Proposition 1** (Blockwise approximation bound). *Assume  $W_{0,ij}$  has no zero entries for every  $(i, j)$ , satisfied by the dense pretrained transformer weights used in our experiments. Then*

$$\inf_{\substack{A_{ij}, B_{ij} \\ \text{rank}(B_{ij} A_{ij}) \leq r_b}} \|\Delta W_{\text{BoHA}} - E\|_F^2 \leq \sum_{i,j=1}^b \|W_{0,ij}\|_{\max}^2 \sum_{k > r_b} \sigma_k^2(R_{ij}), \quad (2)$$

where  $\sigma_k$  are singular values in decreasing order.

HiRA constrains the rank of the full  $R = E \odot W_0$  to the total budget  $r_{\text{tot}}$ . The bound above replaces this global requirement with a per-block rank cap of  $r_b$  at the same total budget  $r_{\text{tot}} = b \cdot r_b$ . Table 1 lists the resulting rank upper bounds for each PEFT family. The synthetic construction in Appendix C gives the extreme case: every block of  $R$  has rank 1 while the full  $R$  has rank  $b^2$ . BoHA at  $r_b = 1$  reconstructs the target to machine precision while HiRA needs global rank at least  $b^2$ . The two bounds tighten under different regimes: BoHA’s bound is tight when each block of  $R$  has rank at most  $r_b$ , while HiRA’s bound is tight when  $R$  has global rank at most  $r_{\text{tot}}$ , including when that rank concentrates within a single block. Empirical comparison across realistic fine-tuning targets follows in the matched-budget single-task and continual-learning diagnostics of Sections 4.4 and 4.3.

A corresponding algebraic update-rank inequality follows from the standard Hadamard rank inequality,  $\text{rank}(P \odot Q) \leq \text{rank}(P) \text{rank}(Q)$  [18]. Applying it to equation 1 with  $C = \bigoplus_{i,j=1}^b B_{ij} A_{ij}$  and using rank subadditivity over the tiled matrix gives  $\text{rank}(C) \leq b^2 r_b = b \cdot r_{\text{tot}}$ . Therefore  $\text{rank}(\Delta W_{\text{BoHA}}) \leq b \cdot \text{rank}(W_0) \cdot r_{\text{tot}}$ , a factor  $b$  above HiRA at matched trainable parameters in Table 1.

**Training and inference.** During training, the base weight  $W_0$  remains frozen and only the block factors  $(A_{ij}, B_{ij})$  are updated. We initialize one factor in each block pair at zero so the initial update is zero. At deployment, BoHA precomputes and merges the blockwise update into the frozen weight on each block as  $W'_{ij} = W_{0,ij} \odot (\mathbf{1} + B_{ij}A_{ij})$ , recovering a single dense matrix  $W'$ . As with LoRA [16] and HiRA [18], inference uses the merged weight directly and introduces no additional inference latency.

**Blockwise gradient locality.** The same partition also determines how gradients reach the adapter factors. Each block sees the corresponding block of the dense layer gradient, weighted elementwise by the frozen pretrained block.

**Proposition 2** (Blockwise gradient locality). *Let  $L$  denote the training loss. Let  $g \in \mathbb{R}^m$  denote the output gradient at a layer and  $x \in \mathbb{R}^n$  its input. Let  $G = gx^\top$  and denote its  $(i, j)$ -block by  $G_{ij}$ . Then*

$$\nabla_{A_{ij}} L = B_{ij}^\top (W_{0,ij} \odot G_{ij}), \quad (3)$$

$$\nabla_{B_{ij}} L = (W_{0,ij} \odot G_{ij}) A_{ij}^\top. \quad (4)$$

The update at block  $(i, j)$  depends only on  $W_{0,ij}$  and  $G_{ij}$ , so a perturbation in input block  $j$  affects only the  $b$  blocks in column  $j$ . By contrast, LoRA’s gradient  $\nabla_A L = B^\top G$  mixes the full outer product through full-matrix factors. This gives a gradient-side analogue of the blockwise approximation argument above.

## 4 Experiments

We evaluate BoHA with a continual-learning diagnostic and matched-budget single-task controls on commonsense and arithmetic reasoning across four base-model scales. The diagnostic tests retention under matched second-task plasticity. The single-task controls assess matched-budget accuracy across task families.

### 4.1 Datasets

**Commonsense reasoning.** We use the eight datasets with predefined train and test splits from LLM-Adapters [17], combining 170,420 query-answer pairs for fine-tuning and reserving 120 entries as a validation set. The eight datasets are BoolQ [5], PIQA [2], SIQA [35], HellaSwag [41], WinoGrande [34], ARC-Challenge and ARC-Easy [6], and OBQA [30]. We evaluate on each dataset independently and report the average across the eight tasks to capture task-specific generalization.

**Arithmetic reasoning.** We fine-tune Mistral-7B [19] and Gemma-2-9B [13] on a 20K-sample subset of MetaMathQA [40], and evaluate on GSM8K [7] and MATH [14], reporting exact-match accuracy consistent with prior work [37].

**Code generation.** We report pass@1 on HumanEval [4] and HumanEval+ in Appendix I.

**Continual-learning diagnostic.** We chain two task families: commonsense  $\rightarrow$  arithmetic (forward) and arithmetic  $\rightarrow$  commonsense (reverse), training each stage from the previous stage’s merged weights. The diagnostic reports stage-1 retention and stage-2 plasticity.

### 4.2 Experimental Settings

**Baselines.** We compare against representative PEFT methods under matched parameter budgets: LoRA [16], DoRA [24], HiRA [18], GraLoRA [20], PiSSA [28], rsLoRA [21], and ABBA [37]. Full fine-tuning (FFT) is included as a full-parameter reference. Our experiments use the Llama-3.2-1B, Llama-3.2-3B [29], Mistral-7B [19], and Gemma-2-9B [13] open-source models.

**Metrics.** For commonsense reasoning, we use accuracy as in HiRA [18] and ABBA [37]. We parse model completions with task-specific answer tokens, mark unmatched responses as incorrect, and report the unweighted average over the eight tasks. Arithmetic benchmarks follow the GSM8K/MATH exact-match protocol after string normalization. For the continual-learning diagnostic, we reuse per-task accuracy and report GEM-style  $R_{i,j}$ , backward transfer, and post-sequence average accuracy [25].

Table 2: Forward continual-learning diagnostic on Llama-3.2-3B.

Method	$R_{1,1}$ (% , $\uparrow$ )	$R_{2,1}$ (% , $\uparrow$ )	$R_{2,2}$ (% , $\uparrow$ )	BWT (% , $\uparrow$ )	ACC (% , $\uparrow$ )
LoRA	81.21	38.55	<u>34.70</u>	-42.66	36.63
DoRA	81.55	40.64	<b>34.86</b>	-40.91	37.75
PiSSA	81.20	36.73	30.36	-44.47	33.55
GraLoRA	82.63	53.81	34.29	-28.81	44.05
ABBA	84.12	53.58	31.76	-30.54	42.67
HiRA	83.27	<u>56.86</u>	31.30	-26.41	<u>44.08</u>
BoHA	<b>84.25</b>	<b>57.66</b>	33.72	<u>-26.59</u>	<b>45.69</b>

**Implementation details.** BoHA uses total rank  $r_{\text{tot}}=32$ . We train for 2 epochs and 1 epoch on the commonsense and arithmetic tasks, respectively. We report the mean accuracy across multiple random seeds for each headline-table configuration. In BoHA, we set  $r_b=r_{\text{tot}}/b$  to exactly match LoRA and HiRA in trainable parameter count and FLOPs. We use  $b=8$ ,  $r_b=4$  in all main comparisons. We use  $\alpha=r_{\text{tot}}=32$  and initialize one factor in each block pair at zero so that the initial update is zero, matching the standard PEFT initialization [16, 18]. As in LoRA and HiRA,  $\alpha$  is a method-internal constant and is not tuned. For BoHA, we use AdamW with learning rate  $2 \times 10^{-3}$  and 100 warm-up steps. Additional implementation details are given in Appendix D.

### 4.3 Results on Continual Learning Diagnostic

We chain the two task families and report the  $2 \times 2$  accuracy matrix  $R_{i,j}$ , where  $R_{i,j}$  is the stage- $i$  model’s accuracy on task  $j$ . The summary metrics are stage-1 retention  $R_{2,1}$ , stage-2 plasticity  $R_{2,2}$ , backward transfer  $\text{BWT} = R_{2,1} - R_{1,1}$ , and post-sequence average  $\text{ACC} = (R_{2,1} + R_{2,2})/2$ . As shown in Table 2 and Figure 3, the Llama-3.2-3B commonsense  $\rightarrow$  arithmetic chain provides the main method-level comparison. BoHA has the highest  $R_{1,1}$ ,  $R_{2,1}$ , and ACC:  $R_{1,1} = 84.25\%$ ,  $R_{2,1} = 57.66\%$ , and  $\text{ACC} = 45.69\%$ . Relative to the  $W_0$ -free additive mean, BoHA gains 15.23% in retained stage-1 accuracy while changing stage-2 accuracy by only 0.17%. HiRA also retains strongly at  $R_{2,1} = 56.86\%$ , while the strongest  $W_0$ -free controls, GraLoRA and ABBA, reach 53.81% and 53.58%. The diagnostic places  $W_0$ -coupled Hadamard adapters at the high-retention end of the design space under matched second-stage plasticity. Reverse-direction scale checks in Appendix H show stronger HiRA/BoHA retention at 9B and no fixed HiRA/BoHA ordering at 1B.

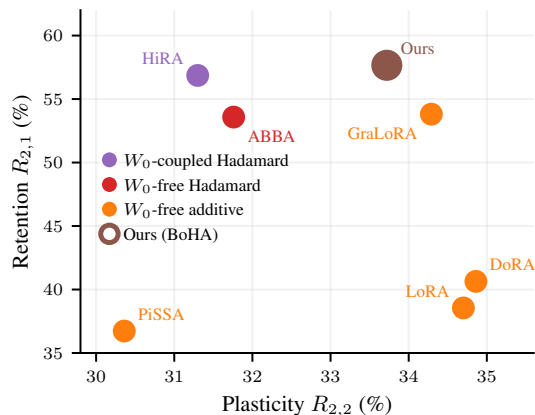


Figure 3: Stability-plasticity trade-off on Llama-3.2-3B forward CL.

### 4.4 Results on Commonsense Reasoning

Table 3 reports matched-budget commonsense results. BoHA improves over the corresponding LoRA row by +1.68 percentage points on Llama-3.2-1B and +3.29 percentage points on Llama-3.2-3B. It matches the FFT average within 0.01 percentage points at both scales while using under 2% of the trainable parameter count. Compared with ABBA, BoHA is below ABBA by 0.14 percentage points at 1B and above ABBA by 0.36 percentage points at 3B, indicating competitive matched-budget single-task capacity within the Hadamard family.

### 4.5 Results on Arithmetic Reasoning

Table 4 reports matched-budget arithmetic results. BoHA reaches 17.97% on Mistral-7B MATH versus ABBA’s 17.96%, and is highest on Gemma-2-9B GSM8K at 79.15%. ABBA is highest on Mistral-7B GSM8K and HiRA is highest on Gemma-2-9B MATH. Across these model and

Table 3: Results (%) on Llama-3.2 1B and 3B across eight commonsense reasoning datasets. The best and second-best PEFT results within each model are indicated in **bold** and underline, respectively. FFT is included as a full-parameter reference. † indicates results taken from ABBA [37].

Model	Method	#Params	Accuracy (↑)								
			OBQA	ARC-c	ARC-e	Wino	HellaS	PIQA	SIQA	BoolQ	Avg.
Llama-3.2-1B	FFT	1.24B	74.00	62.05	78.63	74.79	79.63	80.62	75.37	63.77	73.61
	LoRA	22.54M	71.40	60.49	76.56	72.38	77.41	78.78	73.39	65.11	71.94
	rsLoRA†	22.54M	71.11	59.85	74.90	73.85	75.34	78.32	73.47	<u>65.44</u>	71.54
	DoRA	22.92M	72.20	61.09	76.77	73.01	77.48	78.45	73.34	64.83	72.15
	PiSSA	22.54M	72.20	61.43	77.40	74.03	76.82	79.05	<b>75.54</b>	65.20	72.71
	GraLoRA	22.54M	71.40	60.92	78.54	<u>73.95</u>	77.81	79.87	73.95	65.02	72.68
	ABBA	22.54M	<u>72.93</u>	<u>62.29</u>	<u>79.00</u>	<b>74.74</b>	<b>80.99</b>	<u>80.00</u>	<u>74.75</u>	65.37	<b>73.76</b>
	HiRA	22.54M	70.20	58.70	77.61	71.27	75.74	79.22	73.39	65.26	71.42
	BoHA	22.54M	<b>73.33</b>	<b>62.34</b>	<b>79.89</b>	73.59	<u>79.82</u>	<b>80.59</b>	73.83	<b>65.55</b>	<u>73.62</u>
Llama-3.2-3B	FFT	3.21B	85.00	78.81	90.00	86.55	93.14	87.25	81.49	73.58	84.48
	LoRA	48.63M	79.60	74.32	87.54	83.50	89.63	85.20	79.84	70.00	81.20
	rsLoRA†	48.63M	81.72	74.18	86.71	82.02	90.45	85.05	78.92	69.81	81.11
	DoRA	49.40M	79.80	74.15	88.09	84.14	90.43	85.47	79.84	70.24	81.52
	PiSSA	48.63M	80.80	73.52	86.77	83.24	88.05	84.71	79.43	72.63	81.17
	GraLoRA	48.63M	83.73	76.00	88.90	84.98	92.38	86.53	<u>81.03</u>	72.28	83.23
	ABBA	48.63M	<u>84.27</u>	<u>77.87</u>	<b>89.66</b>	<b>86.53</b>	<b>93.49</b>	<b>87.20</b>	81.00	<u>73.00</u>	<u>84.13</u>
	HiRA	48.63M	83.32	77.61	89.53	85.71	92.94	86.57	80.81	72.83	83.67
	BoHA	48.63M	<b>85.73</b>	<b>78.78</b>	<u>89.62</u>	<u>86.40</u>	<u>93.16</u>	<u>86.69</u>	<b>81.35</b>	<b>74.19</b>	<b>84.49</b>

Table 4: Results (%) on Mistral-7B and Gemma-2-9B across arithmetic reasoning benchmarks. † indicates results taken from ABBA [37].

Method	Mistral-7B			Gemma-2-9B		
	#Params	GSM8K (↑)	MATH (↑)	#Params	GSM8K (↑)	MATH (↑)
FFT†	7.24B	63.87	17.65	9.24B	79.23	38.02
LoRA	83.89M	63.15	15.28	108.04M	76.40	34.68
rsLoRA†	83.88M	62.15	16.24	108.04M	76.84	36.88
DoRA	85.26M	63.76	17.90	109.89M	78.22	37.76
PiSSA†	83.88M	62.43	16.52	108.04M	77.12	37.04
ABBA	83.89M	<b>64.37</b>	<u>17.96</u>	108.04M	78.39	<u>38.50</u>
HiRA	83.89M	62.52	17.31	108.04M	<u>78.44</u>	<b>38.93</b>
BoHA	83.89M	<u>64.11</u>	<b>17.97</b>	108.04M	<b>79.15</b>	38.44

benchmark pairs, BoHA remains close to the strongest Hadamard baseline while improving over LoRA in both base-model settings.

#### 4.6 Training Cost and Memory

Table 5 reports wall-clock and peak memory for matched-budget Llama-3.2-3B commonsense runs using the same batch, sequence length, and two-epoch schedule. Peak memory is identical across LoRA, HiRA, and BoHA in this measurement, consistent with frozen-model activations dominating adapter state at this scale. BoHA matches HiRA’s training time in this implementation and adds 20 minutes 56 seconds over LoRA. BoHA uses one dense weight matrix per adapted projection and introduces no additional inference latency.

## 5 Analysis

The experiments above show that BoHA remains competitive in matched-budget single-task tables. The forward continual-learning diagnostic places  $W_0$ -coupled Hadamard adapters at the high-retention end of the design space. This section analyzes four facets of BoHA’s parameterization:

Table 5: Peak GPU memory and training wall-clock at matched trainable-parameter budget on Llama-3.2-3B commonsense reasoning.

Configuration	Peak GPU memory (GB)	Training wall-clock
LoRA ( $r=32$ )	21.16	3 h 31 m 45 s
HiRA ( $r=32$ )	21.16	3 h 52 m 34 s
BoHA ( $b=8, r_b=4$ )	21.16	3 h 52 m 41 s

the scope of the retention signal, block-count and rank-budget robustness, trained-update spectra, and component placement in the transformer.

### 5.1 Scope of the Retention Diagnostic

The forward continual-learning diagnostic directly compares method-level behavior. On the Llama-3.2-3B commonsense→arithmetic sequence, BoHA achieves  $R_{2,1} = 57.66\%$  and  $R_{2,2} = 33.72\%$  in Table 2, a 15.23% gain in retained stage-1 accuracy over the  $W_0$ -free additive mean while changing stage-2 accuracy by only 0.17%. The same table separates  $W_0$ -coupling and spatial support. HiRA, the  $b=1$  case of BoHA, also retains strongly. GraLoRA is the blockwise  $W_0$ -free control and ABBA is the global  $W_0$ -free Hadamard baseline. The diagnostic supports the  $W_0$ -coupled Hadamard component shared by BoHA and HiRA, while the following subsections examine the blockwise-localization component.

### 5.2 Block Count and Rank-Budget Robustness

Figure 4 reports a rank-budget diagnostic on Llama-3.2-1B, with full per-task results in Table 9. BoHA is above ABBA by 1.62 percentage points at  $r_{\text{tot}}=8$  and 0.69 percentage points at  $r_{\text{tot}}=16$ , and ABBA is above BoHA by 0.14 percentage points at  $r_{\text{tot}}=32$ , supporting low-budget competitiveness within the Hadamard family. At fixed total budget  $r_{\text{tot}} = b r_b$ , smaller  $r_b$  tightens BoHA’s per-block approximation requirement. Table 10 reports the Llama-3.2-3B block-count sweep at  $r_{\text{tot}}=32$ , with BoHA’s average accuracy rising from 83.50% to 83.98% and 84.49% for  $b=2, 4, 8$ . ABBA reaches 84.13% in Table 3, above  $b \in \{2, 4\}$  but below  $b=8$ . We therefore use  $b=8, r_b=4$  in all main results as the strongest tested setting under the shared training protocol.

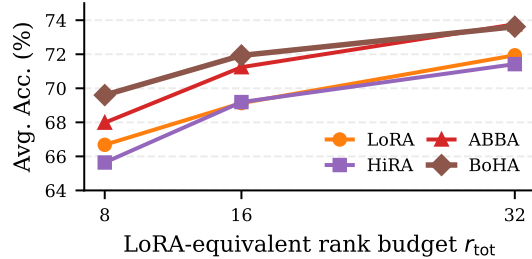


Figure 4: Rank-budget diagnostic on Llama-3.2-1B commonsense reasoning.

### 5.3 Singular Value Structure of Trained Updates

The bounds in Table 1 describe feasible update families. We measure realized spectra of trained updates at Llama-3.2-3B across the seven projections against the FFT proxy  $\bar{E} = W_{\text{FFT}} - W_0$  [18]. Figure 5 reports the entropy-based effective rank [33] per layer. Effective-rank ordering follows the  $W_0$ -coupled versus  $W_0$ -free grouping: the  $W_0$ -coupled methods cluster near FFT, with BoHA at 2083, HiRA at 1982, and FFT at 2130, while the decoupled Hadamard baseline ABBA remains bounded by  $r_1 r_2$  at  $\sim 164$ . BoHA exceeds HiRA in mean effective rank by +19% on  $W_q$ , +7% on  $W_k$ , and +13% on  $W_{\text{gate}}$ , and is tied within  $\pm 1\%$  elsewhere.

Figure 6 reports the count of singular values above 1% of  $\sigma_{\text{max}}$  per layer. LoRA and GraLoRA reach their algebraic ceilings of 32 and 128. For HiRA and BoHA, the algebraic bounds in Table 1 are far above the realized  $\sim 2000$  effective rank, indicating that trained updates concentrate well below the feasible ceiling. The corresponding Frobenius-energy profile is in Appendix J.

### 5.4 Placement of BoHA in Transformers

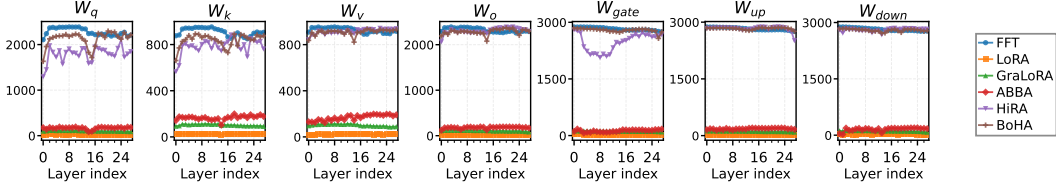


Figure 5: Entropy-based effective rank [33] across layers for FFT, LoRA, GraLoRA, ABBA, HiRA, and BoHA at Llama-3.2-3B.

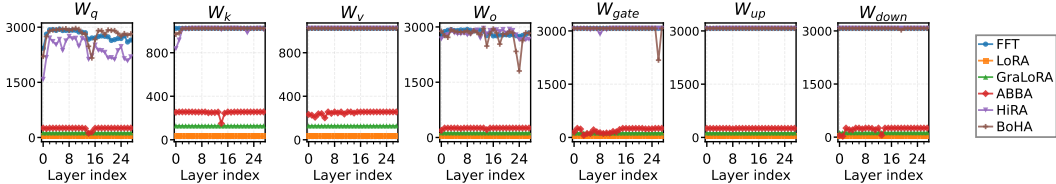


Figure 6: Count of singular values exceeding 1% of the layer-wise maximum for FFT, LoRA, GraLoRA, ABBA, HiRA, and BoHA at Llama-3.2-3B.

Figure 7 and Table 6 report BoHA applied to individual transformer components on Llama-3.2-1B at matched total rank. Among grouped variants, the feed-forward triple (Up, Down, Gate) reaches 73.68%, which is 99.85% of the All-component average of 73.79%, while the joint attention input QKV reaches 69.96%. The strongest single projections are Up at 70.36% and Down at 70.32%, and the weakest are the attention scoring projections Q at 61.95% and K at 62.66%. This ordering is consistent with the placement trend reported by HiRA [18] and ABBA [37], where attention scoring weights contribute the least and representation-transforming weights contribute the most. We use the All-component placement throughout the main-table comparisons of Sections 4.3 and 4.4.

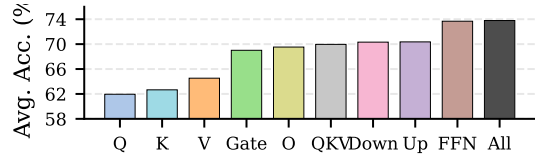


Figure 7: BoHA component-placement diagnostic on Llama-3.2-1B commonsense reasoning at matched total rank.

Table 6: Performance of the Llama-3.2-1B model with BoHA integrated into various components.

Component	OBQA	ARC-c	ARC-e	Wino	HellaS	PIQA	SIQA	BoolQ	Avg. ( $\uparrow$ )
All	73.04	62.66	79.47	74.02	80.35	80.47	74.41	65.91	73.79
FFN	73.10	62.37	79.48	73.90	79.60	81.04	74.16	65.79	73.68
Up	67.80	63.29	67.57	73.37	71.85	75.66	75.17	68.21	70.36
Down	68.80	59.00	76.70	69.97	73.44	77.48	72.68	64.50	70.32
QKV	66.68	57.49	75.64	70.73	75.62	78.01	73.19	62.31	69.96
O	66.52	57.13	75.29	68.92	74.27	78.16	72.36	63.60	69.53
Gate	65.73	57.17	76.25	68.48	71.32	77.37	71.60	64.18	69.01
V	57.95	50.80	69.98	64.39	67.85	76.43	67.90	60.96	64.53
K	58.50	48.98	69.70	63.63	63.21	74.08	65.90	57.32	62.66
Q	57.20	48.55	67.06	65.07	58.54	73.48	64.69	60.99	61.95

## 6 Conclusions

We presented BoHA, a blockwise  $W_0$ -coupled Hadamard product adapter for parameter-efficient fine-tuning that partitions the frozen weight into a  $b \times b$  grid, learns an independent low-rank factorization in each block, and admits a per-block approximation bound and a gradient-locality property. BoHA remains competitive in matched-budget single-task experiments, and the forward matched-plasticity retention diagnostic places  $W_0$ -coupled Hadamard adapters at the high-retention end of the design space, with BoHA retaining more stage-1 accuracy than the  $W_0$ -free additive mean with little change in stage-2 plasticity. These results support blockwise  $W_0$ -coupled Hadamard adaptation as a competitive PEFT design choice when retention under sequential adaptation is part of the objective.

## References

- [1] Armen Aghajanyan, Luke Zettlemoyer, and Sonal Gupta. Intrinsic dimensionality explains the effectiveness of language model fine-tuning. In *Proceedings of the 59th Annual Meeting of the Association for Computational Linguistics (ACL 2021)*, 2021.
- [2] Yonatan Bisk, Rowan Zellers, Ronan Le Bras, Jianfeng Gao, and Yejin Choi. PIQA: Reasoning about physical commonsense in natural language. In *Proceedings of the AAAI Conference on Artificial Intelligence (AAAI 2020)*, 2020.
- [3] Tom B. Brown, Benjamin Mann, Nick Ryder, Melanie Subbiah, Jared Kaplan, Prafulla Dhariwal, Arvind Neelakantan, Pranav Shyam, Girish Sastry, Amanda Askell, Sandhini Agarwal, Ariel Herbert-Voss, Gretchen Krueger, Tom Henighan, Rewon Child, Aditya Ramesh, Daniel M. Ziegler, Jeffrey Wu, Clemens Winter, Christopher Hesse, Mark Chen, Eric Sigler, Mateusz Litwin, Scott Gray, Benjamin Chess, Jack Clark, Christopher Berner, Sam McCandlish, Alec Radford, Ilya Sutskever, and Dario Amodei. Language models are few-shot learners. In *Advances in Neural Information Processing Systems 33 (NeurIPS 2020)*, 2020.
- [4] Mark Chen, Jerry Tworek, Heewoo Jun, Qiming Yuan, Henrique Ponde de Oliveira Pinto, Jared Kaplan, Harri Edwards, Yuri Burda, Nicholas Joseph, Greg Brockman, et al. Evaluating large language models trained on code. *arXiv preprint arXiv:2107.03374*, 2021.
- [5] Christopher Clark, Kenton Lee, Ming-Wei Chang, Tom Kwiatkowski, Michael Collins, and Kristina Toutanova. BoolQ: Exploring the surprising difficulty of natural yes/no questions. In *Proceedings of the 2019 Conference of the North American Chapter of the Association for Computational Linguistics (NAACL-HLT)*, 2019.
- [6] Peter Clark, Isaac Cowhey, Oren Etzioni, Tushar Khot, Ashish Sabharwal, Carissa Schoenick, and Oyvind Tafjord. Think you have solved question answering? try ARC, the AI2 reasoning challenge. *arXiv preprint arXiv:1803.05457*, 2018.
- [7] Karl Cobbe, Vineet Kosaraju, Mohammad Bavarian, Mark Chen, Heewoo Jun, Lukasz Kaiser, Matthias Plappert, Jerry Tworek, Jacob Hilton, Reiichiro Nakano, Christopher Hesse, and John Schulman. Training verifiers to solve math word problems. *arXiv preprint arXiv:2110.14168*, 2021.
- [8] Eric Nuertey Coleman, Luigi Quarantiello, Ziyue Liu, Qinwen Yang, Samrat Mukherjee, Julio Hurtado, and Vincenzo Lomonaco. Parameter-efficient continual fine-tuning: A survey. *CoRR*, abs/2504.13822, 2025. doi: 10.48550/arXiv.2504.13822. URL <https://arxiv.org/abs/2504.13822>.
- [9] Matthias De Lange, Rahaf Aljundi, Marc Masana, Sarah Parisot, Xu Jia, Aleš Leonardis, Greg Slabaugh, and Tinne Tuytelaars. A continual learning survey: Defying forgetting in classification tasks. *IEEE Transactions on Pattern Analysis and Machine Intelligence*, 44(7): 3366–3385, 2022.
- [10] Jacob Devlin, Ming-Wei Chang, Kenton Lee, and Kristina Toutanova. BERT: Pre-training of deep bidirectional transformers for language understanding. In *Proceedings of the 2019 Conference of the North American Chapter of the Association for Computational Linguistics (NAACL-HLT)*, 2019.
- [11] Carl Eckart and Gale Young. The approximation of one matrix by another of lower rank. *Psychometrika*, 1(3):211–218, 1936. doi: 10.1007/BF02288367.
- [12] Ali Edalati, Marzieh Tahaei, Ivan Kobyzev, Vahid Partovi Nia, James J. Clark, and Mehdi Rezagholizadeh. KronA: Parameter efficient tuning with Kronecker adapter. *arXiv preprint arXiv:2212.10650*, 2022.
- [13] Gemma Team. Gemma 2: Improving open language models at a practical size. *arXiv preprint arXiv:2408.00118*, 2024.
- [14] Dan Hendrycks, Collin Burns, Saurav Kadavath, Akul Arora, Steven Basart, Eric Tang, Dawn Song, and Jacob Steinhardt. Measuring mathematical problem solving with the MATH dataset. In *Advances in Neural Information Processing Systems 34 Datasets and Benchmarks Track (NeurIPS 2021)*, 2021.

- [15] Neil Houlsby, Andrei Giurgiu, Stanisław Jastrzebski, Bruna Morrone, Quentin de Laroussilhe, Andrea Gesmundo, Mona Attariyan, and Sylvain Gelly. Parameter-efficient transfer learning for NLP. In *Proceedings of the 36th International Conference on Machine Learning (ICML 2019)*, 2019.
- [16] Edward J. Hu, Yelong Shen, Phillip Wallis, Zeyuan Allen-Zhu, Yuanzhi Li, Shean Wang, Lu Wang, and Weizhu Chen. LoRA: Low-rank adaptation of large language models. In *International Conference on Learning Representations*, 2022.
- [17] Zhiqiang Hu, Lei Wang, Yihuai Lan, Wanyu Xu, Ee-Peng Lim, Lidong Bing, Xing Xu, Soujanya Poria, and Roy Ka-Wei Lee. Llm-adapters: An adapter family for parameter-efficient fine-tuning of large language models. *arXiv preprint arXiv:2304.01933*, 2023.
- [18] Qiushi Huang, Tom Ko, Zhan Zhuang, Lilian Tang, and Yu Zhang. HiRA: Parameter-efficient Hadamard high-rank adaptation for large language models. In *International Conference on Learning Representations*, 2025.
- [19] Albert Q. Jiang, Alexandre Sablayrolles, Arthur Mensch, Chris Bamford, Devendra Singh Chaplot, Diego de las Casas, Florian Bressand, Gianna Lengyel, Guillaume Lample, Lucile Saulnier, L lio Renard Lavaud, Marie-Anne Lachaux, Pierre Stock, Teven Le Scao, Thibaut Lavril, Thomas Wang, Timoth e Lacroix, and William El Sayed. Mistral 7B. *arXiv preprint arXiv:2310.06825*, 2023.
- [20] Yeonjoon Jung, Daehyun Ahn, Hyungjun Kim, Taesu Kim, and Eunhyeok Park. GraLoRA: Granular low-rank adaptation for parameter-efficient fine-tuning. In *Advances in Neural Information Processing Systems 38 (NeurIPS 2025)*, 2025.
- [21] Damjan Kalajdzievski. A rank stabilization scaling factor for fine-tuning with LoRA. *arXiv preprint arXiv:2312.03732*, 2023.
- [22] James Kirkpatrick, Razvan Pascanu, Neil Rabinowitz, Joel Veness, Guillaume Desjardins, Andrei A. Rusu, Kieran Milan, John Quan, Tiago Ramalho, Agnieszka Grabska-Barwinska, Demis Hassabis, Claudia Clopath, Dharshan Kumaran, and Raia Hadsell. Overcoming catastrophic forgetting in neural networks. *Proceedings of the National Academy of Sciences*, 114(13): 3521–3526, 2017.
- [23] Xinlong Li, Weijieying Ren, Wei Qin, Lei Wang, Tianxiang Zhao, and Richang Hong. Analyzing and reducing catastrophic forgetting in parameter efficient tuning. In *ICASSP 2025 – IEEE International Conference on Acoustics, Speech and Signal Processing*, 2025.
- [24] Shih-Yang Liu, Chien-Yi Wang, Hongxu Yin, Pavlo Molchanov, Yu-Chiang Frank Wang, Kwang-Ting Cheng, and Min-Hung Chen. DoRA: Weight-decomposed low-rank adaptation. In *International Conference on Machine Learning*, 2024.
- [25] David Lopez-Paz and Marc’ Aurelio Ranzato. Gradient episodic memory for continual learning. In *Advances in Neural Information Processing Systems 30 (NeurIPS 2017)*, 2017.
- [26] Ilya Loshchilov and Frank Hutter. Decoupled weight decay regularization. In *International Conference on Learning Representations*, 2019.
- [27] Michael McCloskey and Neal J. Cohen. Catastrophic interference in connectionist networks: The sequential learning problem. *Psychology of Learning and Motivation*, 24:109–165, 1989.
- [28] Fanxu Meng, Zhaohui Wang, and Muhan Zhang. PiSSA: Principal singular values and singular vectors adaptation of large language models. In *Advances in Neural Information Processing Systems 37 (NeurIPS 2024)*, 2024.
- [29] Meta AI. Llama 3.2: Revamped lightweight and multimodal models. *Meta AI blog*, 2024. URL <https://ai.meta.com/blog/llama-3-2-connect-2024-vision-edge-mobile-devices/>.
- [30] Todor Mihaylov, Peter Clark, Tushar Khot, and Ashish Sabharwal. Can a suit of armor conduct electricity? a new dataset for open book question answering. In *Proceedings of the 2018 Conference on Empirical Methods in Natural Language Processing (EMNLP)*, 2018.

- [31] Leon Mirsky. Symmetric gauge functions and unitarily invariant norms. *The Quarterly Journal of Mathematics*, 11(1):50–59, 1960.
- [32] Adam Paszke, Sam Gross, Francisco Massa, Adam Lerer, James Bradbury, Gregory Chanan, Trevor Killeen, Zeming Lin, Natalia Gimelshein, Luca Antiga, Alban Desmaison, Andreas Köpf, Edward Yang, Zachary DeVito, Martin Raison, Alykhan Tejani, Sasank Chilamkurthy, Benoit Steiner, Lu Fang, Junjie Bai, and Soumith Chintala. PyTorch: An imperative style, high-performance deep learning library. In *Advances in Neural Information Processing Systems*, 2019.
- [33] Olivier Roy and Martin Vetterli. The effective rank: A measure of effective dimensionality. In *Proceedings of the 15th European Signal Processing Conference (EUSIPCO)*, pp. 606–610, 2007.
- [34] Keisuke Sakaguchi, Ronan Le Bras, Chandra Bhagavatula, and Yejin Choi. WinoGrande: An adversarial Winograd schema challenge at scale. *Communications of the ACM*, 64(9):99–106, 2021.
- [35] Maarten Sap, Hannah Rashkin, Derek Chen, Ronan Le Bras, and Yejin Choi. Social IQa: Commonsense reasoning about social interactions. In *Proceedings of the 2019 Conference on Empirical Methods in Natural Language Processing (EMNLP)*, 2019.
- [36] Reece Shuttleworth, Jacob Andreas, Antonio Torralba, and Pratyusha Sharma. LoRA vs full fine-tuning: An illusion of equivalence. In *Advances in Neural Information Processing Systems 38 (NeurIPS 2025)*, 2025.
- [37] Raghav Singhal, Kaustubh Ponkshe, Rohit Vartak, and Praneeth Vepakomma. ABBA-adapters: Efficient and expressive fine-tuning of foundation models. In *International Conference on Learning Representations*, 2026.
- [38] Thomas Wolf, Lysandre Debut, Victor Sanh, Julien Chaumond, Clement Delangue, Anthony Moi, Pierric Cistac, Tim Rault, Rémi Louf, Morgan Funtowicz, Joe Davison, Sam Shleifer, Patrick von Platen, Clara Ma, Yacine Jernite, Julien Plu, Canwen Xu, Teven Le Scao, Sylvain Gugger, Mariama Drame, Quentin Lhoest, and Alexander M. Rush. Transformers: State-of-the-art natural language processing. In *Proceedings of the 2020 Conference on Empirical Methods in Natural Language Processing: System Demonstrations*, pp. 38–45, 2020.
- [39] Shih-Ying Yeh, Yu-Guan Hsieh, Zhidong Gao, Bernard B. W. Yang, Giyeong Oh, and Yanmin Gong. Navigating text-to-image customization: From LyCORIS fine-tuning to model evaluation. In *International Conference on Learning Representations*, 2024.
- [40] Longhui Yu, Weisen Jiang, Han Shi, Jincheng Yu, Zhengying Liu, Yu Zhang, James T Kwok, Zhenguo Li, Adrian Weller, and Weiyang Liu. Metamath: Bootstrap your own mathematical questions for large language models. *arXiv preprint arXiv:2309.12284*, 2023.
- [41] Rowan Zellers, Ari Holtzman, Yonatan Bisk, Ali Farhadi, and Yejin Choi. HellaSwag: Can a machine really finish your sentence? In *Proceedings of the 57th Annual Meeting of the Association for Computational Linguistics (ACL 2019)*, 2019.
- [42] Qingru Zhang, Minshuo Chen, Alexander Bukharin, Nikos Karampatziakis, Pengcheng He, Yu Cheng, Weizhu Chen, and Tuo Zhao. AdaLoRA: Adaptive budget allocation for parameter-efficient fine-tuning. In *International Conference on Learning Representations*, 2023. URL <https://openreview.net/forum?id=lq62uWRJjiY>.

## Appendix

### A Extended Related Work

**Tensor-product factorisations: KronA and LoKr.** KronA [12] parameterises the update as a Kronecker product  $\Delta W = A \otimes B$  with  $A \in \mathbb{R}^{m_a \times n_a}$ ,  $B \in \mathbb{R}^{m_b \times n_b}$ , and  $m = m_a m_b$ ,  $n = n_a n_b$ . LoKr [39] also low-rank-factorises each Kronecker factor, giving  $\Delta W = (B_1 A_1) \otimes (B_2 A_2)$ . We separate this family from BoHA on two grounds. First, both Kronecker variants are  $W_0$ -free: the trained  $\Delta W$  is added to  $W_0$ , not coupled to it, so they sit in the same  $W_0$ -free row of the design grid as LoRA and ABBA. Second, the Kronecker product imposes a rigid index-tensorised structure: the  $((i_a, i_b), (j_a, j_b))$ -entry of  $A \otimes B$  equals  $A_{i_a j_a} B_{i_b j_b}$ , so every entry is the product of one factor coordinate in  $A$  and one coordinate in  $B$ . BoHA’s per-block Hadamard form  $\Delta W_{ij} = W_{0,ij} \odot (B_{ij} A_{ij})$  does not share this constraint. Blocks are independent, each coupling is element-wise against the corresponding  $W_{0,ij}$ , and the spatial support is a disjoint partition rather than a tensor product. As a consequence, KronA and LoKr capacity scales with the chosen Kronecker factorisation  $(m_a, n_a, m_b, n_b)$  and is not directly commensurate with our  $(b, r_b)$  budget at matched parameter count. KronA and LoKr are therefore placed in the design grid of Figure 1(b) rather than in Tables 3 and 4.

**LoRA-family budget allocation and rank scaling.** AdaLoRA [42] reallocates low-rank budget across weight matrices by importance, and rsLoRA [21] introduces  $\alpha/\sqrt{r}$  scaling. BoHA applies the same scaling convention with per-block rank  $r_b$ , while keeping the rank budget uniform across modules to isolate the spatial-support axis from per-module rank reallocation.

**Approximation bounds and spectral analyses.** HiRA [18] bounds its global approximation error by the  $(r + 1)$ -th singular value of  $E \odot W_0$ , of which Proposition 1 is a direct corollary. Intruder-dimension analysis [36] contrasts LoRA with full fine-tuning but does not compare PEFT families.

**Continual fine-tuning.** Parameter-efficient continual fine-tuning surveys [8] and regulariser-based methods [23] address forgetting through auxiliary mechanisms rather than through the update parameterisation.

### B Detailed Proofs of Propositions 1 and 2

We re-state and prove the two main-body propositions in full. We write  $\|M\|_{\max} = \max_{u,v} |M_{uv}|$  for the entrywise maximum-absolute norm and  $\sigma_k(M)$  for the  $k$ -th singular value of  $M$  in decreasing order.

**Hadamard-Frobenius bound.** For matrices  $A, B \in \mathbb{R}^{p \times q}$  of the same shape,

$$\|A \odot B\|_F^2 \leq \|A\|_{\max}^2 \|B\|_F^2. \quad (5)$$

The bound follows from  $\|A \odot B\|_F^2 = \sum_{u,v} A_{uv}^2 B_{uv}^2 \leq \max_{u,v} A_{uv}^2 \cdot \sum_{u,v} B_{uv}^2 = \|A\|_{\max}^2 \|B\|_F^2$ .

**Proof of Proposition 1.** The placement operator  $\bigoplus$  in equation 1 sends each  $B_{ij} A_{ij}$  to its  $(i, j)$ -tile. Since  $W_0$  and  $E$  admit the conformal partition with blocks  $W_{0,ij}$  and  $E_{ij}$ , the Frobenius norm decomposes as

$$\|\Delta W_{\text{BoHA}} - E\|_F^2 = \sum_{i,j=1}^b \|W_{0,ij} \odot (B_{ij} A_{ij}) - E_{ij}\|_F^2. \quad (6)$$

Under the assumption that  $W_{0,ij}$  has no zero entries,  $R_{ij} = E_{ij} \odot W_{0,ij}$  is well-defined and  $E_{ij} = W_{0,ij} \odot R_{ij}$ . We verified empirically that no entries are exactly zero across the  $q/k/v/o/gate/up/down$  projections of the four pretrained checkpoints used in our experiments (Llama-3.2 1B/3B, Mistral-7B, Gemma-2-9B). The  $(i, j)$ -th term therefore equals  $\|W_{0,ij} \odot (B_{ij} A_{ij} - R_{ij})\|_F^2$ , and equation 5 gives

$$\|W_{0,ij} \odot (B_{ij} A_{ij} - R_{ij})\|_F^2 \leq \|W_{0,ij}\|_{\max}^2 \|B_{ij} A_{ij} - R_{ij}\|_F^2. \quad (7)$$

The factor pairs  $(B_{ij}, A_{ij})$  are unconstrained across blocks, so the per-block infima decouple. By the Eckart-Young-Mirsky theorem [11, 31], the optimal rank- $r_b$  Frobenius approximation to  $R_{ij}$  is its truncated SVD, with residual

$$\inf_{\substack{B_{ij}, A_{ij} \\ \text{rank}(B_{ij}A_{ij}) \leq r_b}} \|B_{ij}A_{ij} - R_{ij}\|_F^2 = \sum_{k > r_b} \sigma_k^2(R_{ij}). \quad (8)$$

Summing over  $(i, j)$  yields equation 2.  $\square$

**Proof of Proposition 2.** Partition the output gradient  $g = [g_1^\top, \dots, g_b^\top]^\top$  with  $g_i \in \mathbb{R}^{m_i}$  and the input  $x = [x_1^\top, \dots, x_b^\top]^\top$  with  $x_j \in \mathbb{R}^{n_j}$  conformally with the row and column splits of  $W_0$ . Then  $G = gx^\top$  has  $(i, j)$ -block  $G_{ij} = g_i x_j^\top$ . By equation 1,  $\Delta W$  on the  $(i, j)$ -tile equals  $W_{0,ij} \odot (B_{ij}A_{ij})$ , and depends only on  $(B_{ij}, A_{ij})$ . Writing  $z = (W_0 + \Delta W)x$  and  $g = \nabla_z L$ , the Frobenius differential of  $L$  at fixed  $(B_{kl}, A_{kl})$  for  $(k, l) \neq (i, j)$  is

$$dL = \langle G_{ij}, W_{0,ij} \odot (dB_{ij}A_{ij} + B_{ij}dA_{ij}) \rangle_F = \langle W_{0,ij} \odot G_{ij}, dB_{ij}A_{ij} + B_{ij}dA_{ij} \rangle_F, \quad (9)$$

where the second equality uses the self-adjointness of the Hadamard product under the Frobenius inner product. Matching against  $dL = \langle \nabla_{B_{ij}} L, dB_{ij} \rangle_F + \langle \nabla_{A_{ij}} L, dA_{ij} \rangle_F$  and applying the matrix-product adjoint identities  $\langle X, Y A^\top \rangle_F = \langle X A, Y \rangle_F$  and  $\langle X, B^\top Y \rangle_F = \langle B X, Y \rangle_F$  yields

$$\nabla_{A_{ij}} L = B_{ij}^\top (W_{0,ij} \odot G_{ij}), \quad \nabla_{B_{ij}} L = (W_{0,ij} \odot G_{ij}) A_{ij}^\top. \quad (10)$$

$\square$

## C Synthetic Reconstruction Sweep

We construct a target update on which BoHA reconstructs exactly at  $r_b=1$  while HiRA’s global approximation matches the construction only at  $r \geq b^2$ . Fix  $m = n = 64$  and  $b = 8$ . All Gaussian draws below use a fixed random seed for reproducibility. Let  $W_0 \in \mathbb{R}^{64 \times 64}$  have i.i.d.  $\mathcal{N}(0, 1)$  entries. For every block  $(i, j)$ , define a rank-1 matrix  $R_{ij} = u_{ij} v_{ij}^\top$  with  $u_{ij}, v_{ij}$  sampled from  $\mathcal{N}(0, I_8)$ , and set  $E_{ij} = W_{0,ij} \odot R_{ij}$ . Then  $\text{rank}(R_{ij}) = 1$  for every block whereas  $\text{rank}(R) = 64$  globally. BoHA at  $r_b = 1$  attains  $\|\Delta W - E\|_F = 2.38 \times 10^{-14}$ . HiRA at the matched per-block budget  $r = 8$  retains error 42.98, and Table 7 shows that it reaches numerical zero only at  $r = b^2 = 64$ .

Table 7: Reconstruction error on the blockwise rank-1 synthetic target ( $m = n = 64$ ,  $b = 8$ ,  $\|E\|_F = 61.37$ ). BoHA at total rank capacity 64 attains numerical zero. HiRA needs  $r = 64$  to match.

Method (config)	Global rank	$\ \Delta W - E\ _F$
HiRA ( $r = 8$ )	8	42.98
HiRA ( $r = 16$ )	16	28.55
HiRA ( $r = 32$ )	32	11.26
HiRA ( $r = 48$ )	48	2.06
HiRA ( $r = 60$ )	60	0.08
HiRA ( $r = 64$ )	64	$1.04 \times 10^{-13}$
<b>BoHA (<math>b = 8, r_b = 1</math>)</b>	<b>64</b>	<b><math>2.38 \times 10^{-14}</math></b>

## D Implementation Details

We implement all methods in PyTorch [32] with HuggingFace Transformers [38]. Experiments run on NVIDIA RTX 5090 32 GB and A100 80 GB GPUs. Base models are loaded in `torch.bfloat16` to reduce memory consumption. Every configuration is trained with the AdamW optimizer [26] with  $\beta_1 = 0.9$ ,  $\beta_2 = 0.999$  and weight decay 0. We train each headline-table configuration with multiple random seeds and report the arithmetic mean across all completed seed runs. Fixed diagnostic runs are reported under their stated protocol.

We configure BoHA on Llama-3.2 1B, Llama-3.2 3B, Mistral-7B, and Gemma-2 9B using the hyperparameters in Table 8. For baseline comparisons, we replicate the experimental setups from

the original LoRA [16], DoRA [24], PiSSA [28], GraLoRA [20], rsLoRA [21], HiRA [18], and ABBA [37] papers to ensure fair and consistent evaluation.

Table 8: Hyperparameter settings of BoHA for training Llama-3.2 1B and 3B on COMMON-SENSE170K, and Mistral-7B and Gemma-2 9B on MetaMathQA.

	Llama-3.2 1B / 3B	Mistral-7B / Gemma-2 9B
Optimizer	AdamW	AdamW
Batch size	6	1
Max. Seq. Len	256	512
Grad Acc. Steps	24	32
Epochs	2	1
Dropout	0.05	0
Learning Rate	$2 \times 10^{-3}$	$2 \times 10^{-3}$
Target Modules	q_proj, k_proj, v_proj, o_proj, gate_proj, up_proj, down_proj	
LR Scheduler	Linear	Cosine
Warmup Ratio	0.02	0.02

For the 2-task continual-learning diagnostic we report the  $2 \times 2$  accuracy matrix  $R_{i,j}$ , where  $R_{i,j}$  is the accuracy of the stage- $i$  model on task  $T_j$  [25]. With  $T_1$  and  $T_2$  the two stages,  $R_{2,1}$ , the *retention* term, is the stage-2 model’s accuracy on the stage-1 task and is our primary diagnostic.  $R_{2,2}$ , the *plasticity* term, is its accuracy on the stage-2 task. From the matrix we derive the standard GEM retention summaries:

$$\begin{aligned} \text{BWT} &= R_{2,1} - R_{1,1} \quad (\text{backward transfer}), \\ F &= \max(0, R_{1,1} - R_{2,1}) = \max(0, -\text{BWT}) \quad (\text{forgetting}), \\ \text{ACC} &= (R_{2,1} + R_{2,2})/2 \quad (\text{post-sequence average}). \end{aligned}$$

$F$  is reported as a non-negative scalar: positive BWT corresponds to backward improvement, negative BWT to forgetting. The pre-registered  $\pm 1\%$  plasticity band applies to the family-level stage-2 gap  $\bar{R}_{2,2}^{(W_0\text{-coupled})} - \bar{R}_{2,2}^{(W_0\text{-free})}$ , averaged within each  $W_0$ -coupling family.

## E Rank-Budget Diagnostic

Table 9 gives the per-task results for the rank-budget diagnostic summarised in Figure 4. The diagnostic varies the LoRA-equivalent rank budget while keeping the same commonsense training and evaluation protocol.

Table 9: Rank-budget diagnostic on Llama-3.2-1B commonsense reasoning. Results are reported as accuracy (%) over the eight sub-tasks and their average.

$r_{\text{tot}}$	Method	OBQA	ARC-c	ARC-e	Wino	HellaS	PIQA	SIQA	BoolQ	Avg.
8	LoRA	62.00	52.73	73.23	68.03	66.48	76.12	71.70	63.12	66.68
	HiRA	59.60	52.90	72.52	65.59	66.06	75.08	70.06	63.33	65.64
	ABBA	64.40	55.20	73.23	68.51	70.12	75.52	73.49	63.33	67.98
	BoHA	67.40	56.91	76.30	68.98	73.10	77.15	72.52	64.40	<b>69.60</b>
16	LoRA	65.40	57.25	74.71	69.93	72.80	76.55	72.62	63.79	69.13
	HiRA	66.80	56.40	75.80	68.67	71.78	77.64	71.75	64.71	69.19
	ABBA	67.80	59.22	76.64	71.82	77.44	78.94	73.29	64.77	71.24
	BoHA	72.00	59.30	78.91	70.88	77.13	78.45	73.85	64.92	<b>71.93</b>
32	LoRA	71.40	60.49	76.56	72.38	77.41	78.78	73.39	65.11	71.94
	HiRA	70.20	58.70	77.61	71.27	75.74	79.22	73.39	65.26	71.42
	ABBA	72.93	62.29	79.00	74.74	80.99	80.00	74.75	65.37	<b>73.76</b>
	BoHA	73.33	62.34	79.89	73.59	79.82	80.59	73.83	65.55	73.62

Table 10 gives the block-count sweep referenced in Section 5.2. The sweep keeps the LoRA-equivalent total rank fixed and varies the number of blocks. The  $b=8$  row is the canonical main-result setting.

Table 10: Block-count sweep on Llama-3.2-3B commonsense reasoning at fixed total rank  $r_{\text{tot}} = 32$ .

$b$	$r_b$	$r_{\text{tot}}$	Avg. Acc. (%)
2	16	32	83.50
4	8	32	83.98
8	4	32	84.49

## F Equivalence at $b=1$

Setting  $b=1$  collapses the BoHA partition to a single block and recovers the HiRA parameterization. We evaluate this equivalence with a paired Llama-3.2-1B comparison. The BoHA–HiRA average-accuracy gap is +0.05 percentage points. The associated paired  $t$ -test gives  $p = 0.8868$ , placing the residual within the bf16 and Kaiming-initialization seed variability of this paired run. This agreement is consistent with the algebraic reduction and separates the  $b=1$  endpoint from the  $b > 1$  blockwise settings studied in the block-count and rank-budget controls.

## G Additional Results on Arithmetic Reasoning

We evaluate BoHA on a 40K-sample subset of MetaMathQA at Mistral-7B and Gemma-2-9B, doubling the data budget of the main 20K comparison. Results are reported in Table 11. BoHA exceeds the FFT reference from ABBA on both Mistral-7B metrics and on Gemma-2-9B GSM8K. Among the reported PEFT rows, BoHA leads on three of four metric cells, with HiRA leading on Gemma-2-9B MATH at 40.02% versus BoHA’s 38.58%.

Table 11: Results (%) on Mistral-7B and Gemma-2-9B across arithmetic reasoning benchmarks (GSM8K and MATH) on the MetaMathQA-40K subset.  $\dagger$  indicates results taken from ABBA [37].

Method	Mistral-7B			Gemma-2-9B		
	#Params	GSM8K ( $\uparrow$ )	MATH ( $\uparrow$ )	#Params	GSM8K ( $\uparrow$ )	MATH ( $\uparrow$ )
FFT $\dagger$	7.24B	66.28	18.34	9.24B	79.89	39.44
LoRA	83.89M	64.44	16.92	108.04M	76.95	34.84
ABBA	83.89M	65.35	18.16	108.04M	79.83	<u>38.82</u>
HiRA	83.89M	66.19	18.76	108.04M	79.91	<b>40.02</b>
BoHA	83.89M	<b>66.87</b>	<b>19.98</b>	108.04M	<b>80.44</b>	38.58

## H Reverse-direction continual learning diagnostic

Table 12: Reverse-direction continual-learning diagnostic (arithmetic  $\rightarrow$  commonsense) on Llama-3.2-1B and Gemma-2-9B. Reverse cells are single-seed runs that serve as a direction and scale check rather than a fully replicated comparison.

Model	Method	$R_{1,1}$ (% , $\uparrow$ )	$R_{2,1}$ (% , $\uparrow$ )	$R_{2,2}$ (% , $\uparrow$ )	BWT (% , $\uparrow$ )	ACC (% , $\uparrow$ )
Llama-3.2-1B	LoRA	<u>16.63</u>	3.12	<u>63.53</u>	-13.51	<u>33.33</u>
	ABBA	14.13	<u>3.49</u>	60.20	-10.64	31.85
	HiRA	15.50	<b>3.70</b>	59.58	-11.80	31.64
	BoHA	<b>17.10</b>	3.40	<b>65.05</b>	-13.70	<b>34.23</b>
Gemma-2-9B	LoRA	55.87	10.46	86.97	-45.41	48.72
	ABBA	58.83	18.37	<u>88.48</u>	-40.46	53.42
	HiRA	<u>58.85</u>	<b>27.54</b>	87.84	-31.31	<b>57.69</b>
	BoHA	<b>59.09</b>	<u>21.85</u>	<b>88.97</b>	-37.24	<u>55.41</u>

Table 12 reports the reverse-direction continual-learning diagnostic for Llama-3.2-1B and Gemma-2-9B as a direction and scale check on the forward 3B finding. At Gemma-2-9B reverse, the family ordering replicates the forward 3B grouping: HiRA and BoHA reach the highest stage-1 retention at

$R_{2,1}$  of 27.54% and 21.85%, ABBA sits between the coupled pair and LoRA at 18.37%, and LoRA falls last at 10.46%. The cross-family ordering between  $W_0$ -coupled and  $W_0$ -free PEFT updates is consistent with the 3B forward grouping. At Llama-3.2-1B reverse, all four methods compress into an  $R_{2,1}$  band between 3% and 4% where the gaps fall within evaluation noise, so we treat the 1B reverse ranking as inconclusive. Within the  $W_0$ -coupled family the BoHA versus HiRA order varies with scale and direction: BoHA leads in 3B forward, HiRA leads BoHA by 5.69% in 9B reverse, and HiRA leads BoHA in 1B reverse. The within-family ordering is therefore scale-dependent, while the cross-family separation between  $W_0$ -coupled and  $W_0$ -free PEFT updates is the signal emphasized in the main text.

## I Code Generation Evaluation

As shown in Table 13, BoHA achieves the best pass@1 on three of four metric cells, leading at Llama-3.2-1B on both HumanEval and HumanEval+ and at Llama-3.1-8B on HumanEval. These results suggest that BoHA’s gains are not confined to reasoning. The two-model scope follows HiRA [18] and ABBA [37], which report code generation on the same two models.

Table 13: Code-generation pass@1 (%) on HumanEval and its EvalPlus-augmented variant HumanEval+ at Llama-3.2-1B and Llama-3.1-8B.

Method	Llama-3.2-1B		Llama-3.1-8B	
	HumanEval (↑)	HumanEval+ (↑)	HumanEval (↑)	HumanEval+ (↑)
LoRA	25.6	22.0	56.7	53.7
ABBA	25.0	22.6	54.9	50.0
HiRA	25.0	22.6	56.1	51.8
BoHA	26.2	24.4	57.3	52.4

## J Frobenius Energy of Trained Updates

We report the unnormalised Frobenius energy  $\|\Delta W\|_F^2$  of trained updates as a companion diagnostic to the effective rank and 1%-threshold counts of Section 5.3. Both rank diagnostics there cluster methods by  $W_0$ -coupling and structural family. The energy diagnostic decouples from those orderings and is dominated by adapter scaling conventions rather than by spectral breadth.

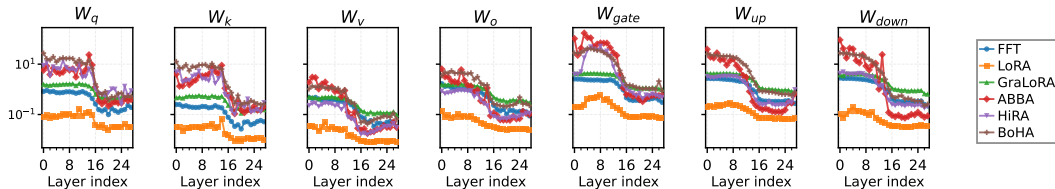


Figure 8: Layer-wise sum of squared singular values for FFT, LoRA, GraLoRA, ABBA, HiRA, and BoHA at Llama-3.2-3B on a log-y axis.

Figure 8 reports this diagnostic layer by layer on Llama-3.2-3B. The mean ordering on  $\|\Delta W\|_F^2$  is ABBA > BoHA > HiRA > GraLoRA > FFT > LoRA across the seven trained projections. The curves therefore follow a different ordering from the effective-rank diagnostics in Figure 5 and Figure 6. All multiplicatively-scaled adapters sit above FFT in absolute energy because their parameterisations include  $\alpha$ -based scaling factors not present in the FFT update. ABBA has the highest energy mean, but its effective rank in Figure 5 remains mid-range at approximately 164, showing that unnormalised energy alone does not predict spectral breadth. BoHA’s and HiRA’s proximity to FFT in effective rank is consistent with the  $W_0$ -coupled design.